Environmental Science & Technology

pubs.acs.org/est

Article

Visible-Light Activation of a Dissolved Organic Matter–TiO_2 Complex Mediated *via* Ligand-to-Metal Charge Transfer

Hoang Tran Bui,[⊥] Hyeon Yeong Park,[⊥] Pedro J. J. Alvarez, Jaesang Lee,* Wooyul Kim,* and Eun-Ju Kim*

Cite This: *Environ. Sci. Technol.* 2022, 56, 10829–10837

Read Online

ACCESS | Metrics & More | Article Recommendations | Supporting Information

ABSTRACT: Given the widespread use of TiO_2, its release into aquatic systems and complexation with dissolved organic matter (DOM) are highly possible, making it important to understand how such interactions affect photocatalytic activity under visible light. Here, we show that humic acid/TiO_2 complexes (HA/TiO_2) exhibit photoactivity (without significant electron–hole activation) under visible light through ligand-to-metal charge transfer (LMCT). The observed visible-light activities for pollutant removal and bacterial inactivation are primarily linked to the generation of H_2O_2 *via* the conduction band. By systematically considering molecular-scale interactions between TiO_2 and organic functional groups in HA, we find a key role of phenolic groups in visible-light absorption and H_2O_2 photogeneration. The photochemical formation of H_2O_2 in river waters spiked with TiO_2 is notably elevated above naturally occurring H_2O_2 generated from background organic constituents due to LMCT contribution. Our findings suggest that H_2O_2 generation by HA/TiO_2 is related to the quantity and functional group chemistry of DOM, which provides chemical insights into photocatalytic activity and potential ecotoxicity of TiO_2 in environmental and engineered systems.

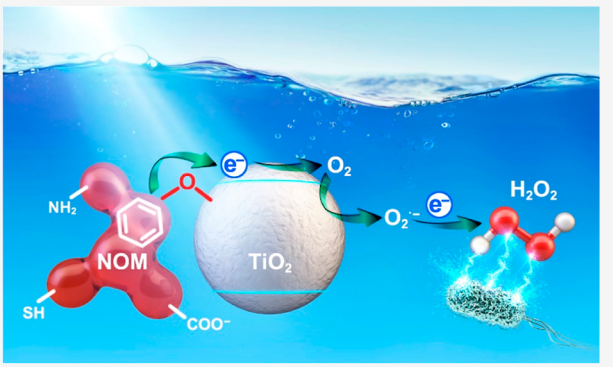

KEYWORDS: *titanium dioxide nanoparticles, humic acid, ligand-to-metal charge transfer (LMCT), visible light, hydrogen peroxide*

INTRODUCTION

Titanium dioxide (TiO_2) comprises a high fraction of nanoparticle production[1−5] due to its widespread use in consumer and industrial products. Potential environmental impacts of TiO_2 have been widely assessed under UV illumination because titania, a wide band-gap semiconductor (3.0−3.2 eV), only absorbs UV light (<5% of sunlight).[6−8] However, limited attention has been given to the effects of nTiO_2 upon exposure to visible light in the presence of photosensitizing dissolved organic matter (DOM) that abounds in natural waters.

Photosensitization is an effective approach to extend the photoresponse of TiO_2 to the visible-light region.[9−17] Two types of photosensitization processes may be used: dye sensitization and ligand-to-metal charge transfer (LMCT) sensitization.[9] Dye sensitization occurs *via* the highest occupied molecular orbital (HOMO)−lowest unoccupied molecular orbital photoexcitation of a dye, followed by an electron transfer from the dye-excited state to the conduction band (CB) of TiO_2, while the LMCT sensitization involves a visible-light-induced electron transfer from the HOMO of adsorbates to the TiO_2 CB (Scheme S1). Unlike dye sensitization where the dye must absorb visible light, the adsorbate in LMCT sensitization does not have to absorb visible light.[9] Various organic and inorganic compounds with diverse functionalities have been used to form visible light-responsive LMCT complexes with TiO_2.[10,12−14]

DOM is characterized by a large mixture of organic molecules containing carboxyl, phenolic, hydroxyl, quinone, and nitrogen- and sulfur-containing functional groups, some of which are chromophores.[18] Given the favorable adsorption of DOM onto TiO_2 surfaces through electrostatic attraction and ligand exchange,[19] DOM is likely to form LMCT complexes on TiO_2. The molecular structure of a ligand determines the binding mode to the TiO_2 surface, which in turn, affects the electronic coupling strength. For example, catechol formed relatively strong electronic coupling with TiO_2 compared to salicylate.[20] We postulate that the mechanism of reactive oxygen species (ROS) generation varies depending on the electronic coupling of the ligand with TiO_2. Controlling the ROS formation [mainly, singlet oxygen ($^1O_2$), superoxide

Received: April 26, 2022
Revised: June 17, 2022
Accepted: June 21, 2022
Published: June 29, 2022

anion radical ($^{\bullet}O_2^-$), hydrogen peroxide (H_2O_2), and hydroxyl radical ($^{\bullet}OH$)] in the photocatalytic system is critical because these species are implicated in a variety of processes in aquatic environments, including degradation of organic pollutants and inactivation of bacteria and viruses,[21,22] as well as ecotoxicity.[23,24] However, the ligand heterogeneity of DOM often hinders the determination of the exact role of specific functional groups in surface complexation with TiO_2. Thus, understanding complexation at the molecular level could provide valuable insight into DOM chemistry that controls LMCT sensitization and ROS generation.

The present study reports that humic acids (HAs) can form a LMCT band on the TiO_2 surface (from ca. 400 nm to ca. 650 nm), which enables the TiO_2/HA complex (HA/TiO_2) to harvest the visible light successfully. The remarkable performance of HA/TiO_2 for the removal of various pollutants and the inactivation of waterborne bacteria is ascribed to the enhanced generation of ROS, mainly H_2O_2 under visible-light irradiation (λ > 420 nm). These results infer the involvement of the CB electron-induced reduction process only in the LMCT sensitization, thus minimizing the oxidative consumption of H_2O_2 by photogenerated valence band holes. To probe the role of HA chemistry in the LMCT process as an alternative sensitization, we further evaluate the visible-light absorption and H_2O_2 generation of TiO_2−organic ligand complexes. The data presented here focus on the simple functional groups of HA as a starting point and highlight the importance of the quantity and composition of DOM in controlling H_2O_2 generation in the photocatalytic system.

MATERIALS AND METHODS

Materials. The following reagent-grade chemicals were used: 4-chlorophenol (4-CP, Sigma-Aldrich), *N*,*N*-diethyl-1,4-phenylene-diamine sulfate (DPD, Sigma-Aldrich), horseradish peroxidase (Sigma-Aldrich), phosphoric acid solution (Sigma-Aldrich), 2,3-bis-(2-methoxy-4-nitro-5-sulfophenyl)-2*H*-tetrazolium-5-carboxanilide (XTT, Sigma-Aldrich), sodium dichromate dihydrate ($Na_2Cr_2O_7$.$2H_2O$, Sigma-Aldrich), *tert*-butyl alcohol (TBA, Sigma-Aldrich), 1,5-diphenylcarbazide (DPC, Sigma-Aldrich), sodium perchlorate ($NaClO_4$, Sigma-Aldrich), aniline (Sigma-Aldrich), phthalic acid (Sigma-Aldrich), thiophenol (Sigma-Aldrich), pyrocatechol (Sigma-Aldrich), sodium dichloroacetate (DCA, Sigma-Aldrich), 5,5-dimethyl-1-pyrroline *N*-oxide (DMPO, Sigma-Aldrich), coumarin (Sigma-Aldrich), sodium fluoride (NaF, Sigma-Aldrich), superoxide dismutase (SOD, Sigma-Aldrich), catalase (CAT, Sigma-Aldrich), dibasic sodium phosphate heptahydrate (Samchum), monobasic sodium phosphate (Kanto), 3′-(*p*-hydroxyphenyl)-fluorescein (HPF, Thermo Fisher), and hydrogen peroxide solution (H_2O_2, Junsei). TiO_2 (Evonik Degussa P25) and Suwannee River HA [SRHA, International Humic Substances Society (IHSS)] were used in all the experiments. The HA concentration was measured as dissolved organic carbon using a total organic carbon analyzer (Shimadzu TOC-LCPH E200 ROHS). *Escherichia coli* (KCTC 2571) was supplied by the Korean Collection for Type Culture (KCTC). All solutions and suspensions were prepared using ultrapure deionized water (>18 MΩ·cm), produced by a Barnstead purification system (Thermo Scientific). The river water sample was collected from the Han River in Yangpyeong (Korea) and filtered through a 0.45 μm membrane (Millipore). A summary of the river water physicochemical characteristics is provided in Table S1.

Photocatalytic Experiments and Sample Analysis. Photocatalytic experiments were conducted in a 30 mL pyrex reactor with a quartz window (40 mm diameter) containing aqueous suspensions of TiO_2, HA, and target pollutants (4-CP, Cr(VI), DCA, or *E. coli*) at pH 3 (±0.05) under visible-light irradiation. The external light was provided by a 300 W Xe arc lamp (Oriel) equipped with a 10 cm IR water filter and a cutoff filter (λ > 320 nm and λ > 420 nm for UV and visible-light irradiations, respectively), and the typical incident light intensity was determined to be approximately 100 mW cm^{-2}. Simulated sunlight was provided by an AM 1.5 G solar simulator (Oriel). Prior to irradiation, the suspension was stirred in the dark for 20 min to ensure adsorption equilibrium. Sample aliquots were withdrawn from the reactor at predetermined time intervals using a 1 mL syringe and filtered through a 0.45 μm PTFE filter (Millipore). The degradation of 4-CP was monitored using a high-performance liquid chromatography (Shimadzu, LC-20AD pump) system combined with a diode array detector and a Shim-pack GIS column (4.6 mm × 250 mm). A mixture of 0.1% H_3PO_4 solution and can at 60:40 was used as the eluent. The reduction of Cr(VI) was analyzed by the colorimetric DPC method. The absorption of the Cr−DPC complex at 540 nm was monitored using a UV−vis spectrophotometer (Sinco S-3100).[25] Quantification of DCA was performed using an ion chromatograph (Thermo Dionex Aquion)-conductivity detector combined with a Dionex IonPac AS 22 (4 mm × 150 mm) column. The eluent solution was 3.5 mM Na_2CO_3/1 mM $NaHCO_3$. Bacterial inactivation efficiency was determined by counting the colonies on agar plates before and after treatment.

Characterizations. TiO_2 samples were characterized before and after HA adsorption using scanning electron microscopy (SEM, Hitachi Regulus 8230), X-ray diffraction (XRD, Bruker D8-ADVANCE), X-ray photoelectron spectroscopy (XPS, ULVAC-PHI PHI 5000 Versa Probe system), and Fourier transform infrared (FTIR) spectroscopy (Bruker Vertex 80v). The optical absorption spectra of the HA, TiO_2, and TiO_2/HA complex (HA/TiO_2) powders were recorded using a diffuse reflectance UV−vis spectrophotometer (DR−UVS). Photocurrent generation was measured using a TiO_2/FTO electrode prepared by the doctor blade method in 0.5 M $NaClO_4$ at pH 3. The TiO_2/FTO, Pt, and Ag/AgCl electrodes were used as working, counter, and reference electrodes, respectively. The HA solution was spiked in the electrolyte three times to gradually increase its concentration (2.5, 5, and 10 mg/L). Photocurrents were measured at a constant potential (0.145 V) using a potentiostat (Metrohm AG). Steady-state photoluminescence (PL) spectra were recorded on a fluorescence spectrophotometer (Hitachi F-7000) with an excitation wavelength of 400 nm. Time-resolved PL decay traces were obtained by a time-correlated single-photon counting system (PicoQuant Fluotim 200) with a 1 MHz repetition rate. The samples were excited by a 375 nm laser source, and the emitted PL was collected by a photon multiplier tube detector (PicoQuant PMA 182) at 550 nm.

ROS Quantification. The production of $^{\bullet}OH$ was monitored by fluorescence measurements using HPF and coumarin as $^{\bullet}OH$ trapping agents. The fluorescence emission intensity of HPF was measured using a spectrofluorometer (JASCO, FP-8500) at 515 nm following excitation at 490 nm. Fluorescence emission of 7-hydroxycoumarin, a hydroxylated product of coumarin, was measured at 460 nm following excitation at 332 nm. The quantitative analyses of $O_2^{\bullet-}$ and

https://doi.org/10.1021/acs.est.2c02975
Environ. Sci. Technol. 2022, 56, 10829−10837

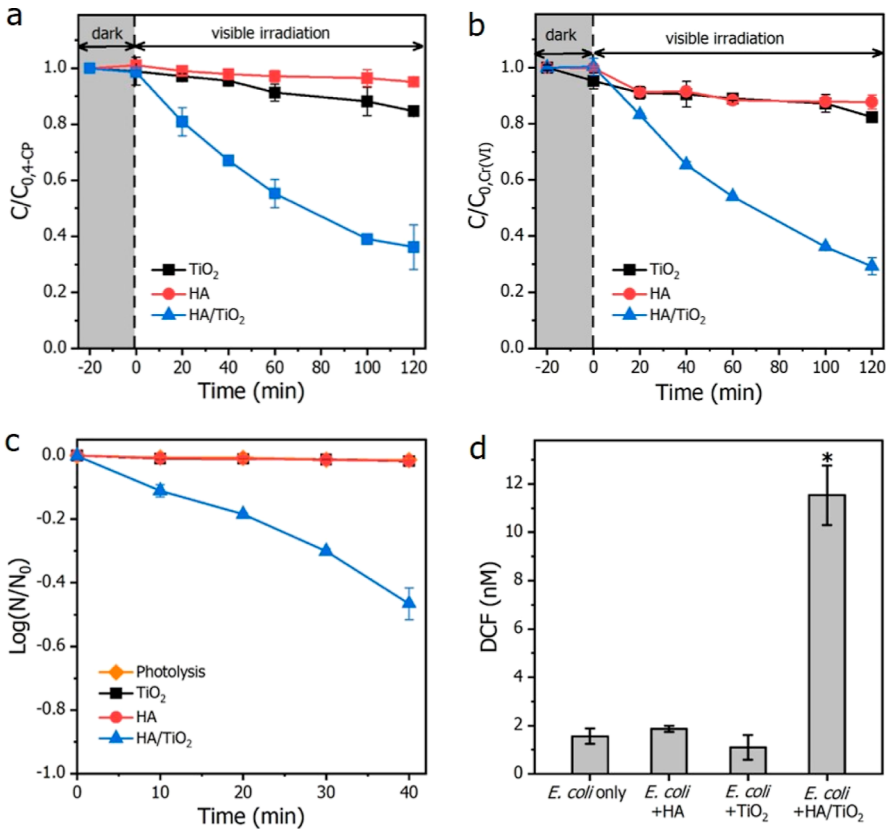

Figure 1. (a) Degradation of 4-CP, (b) reduction of Cr(VI), and (c) inactivation of *E. coli* by TiO_2, HA, and HA/TiO_2 under visible-light irradiation. (d) Intracellular ROS production evaluated by DCF fluorescence in *E. coli* (*$p < 0.05$ vs cell control). Experimental conditions: [TiO_2] = 0.5 g L^{-1}; [HA] = 10 mg L^{-1}; $[4\text{-CP}]_0$ = 100 μM; $[Cr(VI)]_0$ = 200 μM; $[E.\ coli]_0 = 10^7$ CFU mL^{-1}; pH_i = 3; λ > 420 nm; air-equilibrated.

H_2O_2 were performed on a UV−vis spectrophotometer, using the XTT-formazan production and DPD methods, respectively.[26,27] Electron paramagnetic resonance (EPR) spectroscopy (Bruker ELEXYS E580) was employed to detect the ROS captured by the DMPO reagent.

Statistical Analyses. All experiments were performed in triplicate (or more replicates), and Student's *t*-test (two-tailed) was used to determine if the differences were significant (i.e., $p < 0.05$). Data were presented as mean ± standard deviation.

RESULTS AND DISCUSSION

Visible-Light Activity of HA/TiO_2. Control tests with either TiO_2 or HA alone did not significantly remove 4-CP, Cr(VI), and *E. coli* under visible light (Figure 1a−c)—except for a small amount of 4-CP removed by visible-light-illuminated TiO_2, which was likely facilitated by direct electron transfer from adsorbed 4-CP to the TiO_2 CB.[28] In contrast, HA/TiO_2 exhibited remarkable visible-light activities for 4-CP degradation, reduction of Cr(VI) to Cr(III), and *E. coli* inactivation (Figure 1a−c). After 2 h of irradiation, the removal of TOC associated with 4-CP reached 55% in the HA/TiO_2 suspension, compared to only 10% for TiO_2 alone, suggesting that some 4-CP was mineralized by HA/TiO_2 under visible light. In addition, significant photoreduction of Cr(VI) by HA/TiO_2 was achieved even in the presence of O_2, another electron acceptor. This is likely related to the fact that Cr(VI) reduction is thermodynamically more favorable than that of O_2.[29]

We ruled out the possibility that UV light leaking from the cutoff filter may contribute to the observed pollutant removal, given the negligible degradation of DCA in visible light (Figure S1). Therefore, the mechanism of organic degradation and bacterial inactivation by HA/TiO_2 under visible-light irradiation must be different from that under UV light, which is known to involve OH radicals. To verify this, we examined the effect of TBA as an OH radical scavenger on the degradation of 4-CP by HA/TiO_2 under UV or visible-light irradiation (Figure S2). TBA significantly hindered 4-CP degradation under UV light but had little impact under visible light, which infers that 4-CP degradation under visible light occurred *via* a different pathway not involving OH radicals.

A photocatalytic reaction typically causes oxidative stress in bacterial cells owing to the generation of ROS, which leads to cellular damage and ultimately cell death.[30] To address the relationship between visible-light-induced bactericidal activity and oxidative stress, we probed the ROS level in *E. coli* using a fluorescent probe (H2DCFDA). The generation of intracellular ROS was significant only in cells treated with HA/TiO_2 (Figure 1d). These results demonstrate that HA/TiO_2 can exert oxidative stress under visible light, resulting in the observed cytotoxicity to *E. coli*.

Formation of the Visible-Light-Absorbing Surface Complex. Adsorption of HA on TiO_2 is a requirement for efficient electron transfer. The HA adsorption isotherm on TiO_2 at pH 3 is shown in Figure S3a. At pH 3, almost all of the HAs were adsorbed on TiO_2 in the range of 2.5−20 mg/L HA, as shown by the linear portion of the curve. The net surface charge of TiO_2 and HA was opposite at low pH, as indicated by zeta potential measurements (Figure S3b). This results in electrostatic attraction that enhances HA adsorption onto

https://doi.org/10.1021/acs.est.2c02975
Environ. Sci. Technol. 2022, 56, 10829−10837

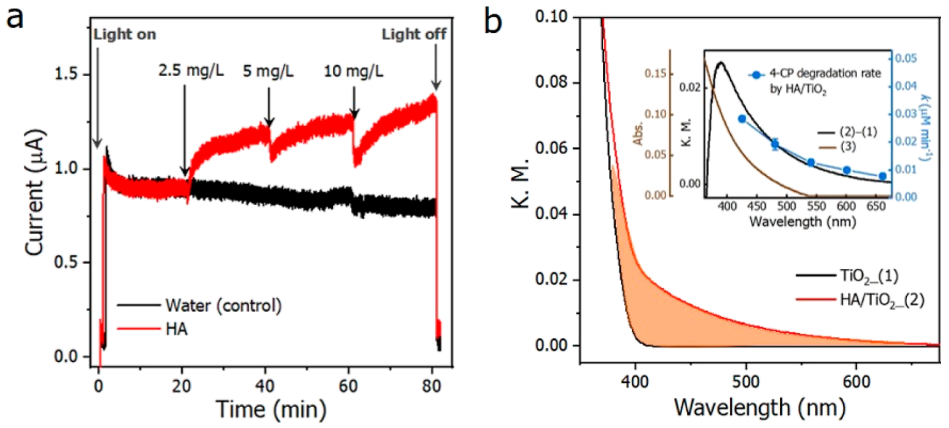

Figure 2. (a) Photocurrent time profiles obtained with a TiO_2 photoanode in response to the spike of HA (from 2.5 to 10 mg L^{-1}) and water (the same volume with HA added). Experimental conditions: [$NaClO_4$] = 0.5 M; applied potential of +0.145 V (vs Ag/AgCl); λ > 420 nm; air-equilibrated; pH_i = 3. (b) DR UV−vis spectra of TiO_2 and HA/TiO_2 at pH 3. The colored area shows the range of LMCT transition. Inset: difference spectrum (2 − 1); UV−vis absorption spectrum of HA (3); wavelength-dependent activity of HA/TiO_2 for 4-CP degradation. The ordinate scale in the DR spectra is expressed in Kubelka−Munk units. The experimental conditions for 4-CP degradation were the same as for Figure 1a.

TiO_2. However, HA adsorption propensity decreases at near-neutral pH as the magnitude of the opposing zeta potentials of TiO_2 and HA decrease significantly (Figure S3b). The observed decrease in 4-CP and Cr(VI) removal efficiency by visible-illuminated HA/TiO_2 at pH 6 compared to pH 3 (Figure S4) corroborates the importance of adsorption of HA onto the TiO_2 surface in the process.

SEM images (Figure S5a,b) and XRD patterns (Figure S5c) of TiO_2 and HA/TiO_2 showed that HA adsorption did not induce a morphological change or phase transformation in the bare TiO_2. HA/TiO_2 exhibited a BET surface area of 53 m^2/g, which was not significantly affected by HA adsorption compared to that of bare TiO_2 (56 m^2/g). The chemical interaction between HA and TiO_2 was investigated by XPS analysis. The high-resolution C 1s spectrum of HA/TiO_2 could be resolved into three peaks, corresponding to C═C (284.6 eV), C−O (285.6 eV), and O−C═O (288.4 eV) (Figure S5d). The high-resolution O 1s spectrum corroborated with the data for the C 1s spectrum and revealed the presence of the peak at 529.5 eV (Figure S5e) attributed to Ti−O−C,[31] indicating the importance of such bonds in the surface complex formation between HA and TiO_2. The formation of the HA−TiO_2 complex through ligand adsorptions of phenolic and carboxylic groups was further supported by the occurrence of several prominent peaks at 1060, 1380, 1450, and 1610 cm^{-1} in the FTIR spectrum (Figure S5f), which can be assigned to C−O stretching of alcohol functional groups, C−O stretching of phenolic OH groups, aromatic C−C bands, and COO asymmetric stretching.

The photocurrent generated as a function of HA concentration was monitored at the TiO_2/FTO electrode under visible-light irradiation. Substantially higher currents were observed during visible-light illumination with HA than without HA (Figure 2a). Moreover, the gradual increase in the photocurrent intensity with the HA concentration might come from electron transfer from adsorbed HA to the TiO_2 CB. Steady-state and time-resolved PL measurements were performed to gain additional insight into the electron transfer between HA and TiO_2. Figure S6a shows a strongly quenched PL emission of HA in the presence of TiO_2. The PL intensity of HA decreased more significantly with increasing TiO_2 concentrations, indicative of the promoted electron transfer from HA to the TiO_2 CB. Since HA serves as an electron donor in our system, HA may be oxidized and degraded. However, we could not detect any sign of HA degradation during visible-light irradiation (Figure S7), which is related to the supramolecular structure of HA that has comparable electron-accepting/donating capacity.[32] The time-resolved decay profile of HA and HA/TiO_2 in Figure S6b could be fitted with a biexponential or triexponential function (Table S2). The average PL lifetimes for HA and HA/TiO_2 were calculated to be ∼1.3 and 0.6 ns, respectively. The shortened average lifetime and the emergence of an additional fast component (τ_1) in HA/TiO_2 corroborate the interfacial electron transfer between HA and TiO_2.

The DR UV−vis absorption spectra of TiO_2 and HA/TiO_2 at pH 3 and pH 6.6 revealed similar absorption patterns (Figures 2b and S8). In contrast to TiO_2 that showed no absorption signature in the visible range, HA/TiO_2 exhibited a broad absorption in the region of λ > 400 nm tailing to around 650 nm (Figures 2b and S8). The absorption pattern of HA alone exhibited an exponential decrease in absorbance with increasing wavelength and almost no absorbance above 500 nm (inset of Figure 2b). Thus, the more pronounced absorption of HA/TiO_2 in the lower-energy region can be attributed to the LMCT transition from the adsorbed HA to Ti(IV) on the TiO_2 surface. In support of this explanation, the visible-light absorption was obviously decreased when the HA/TiO_2 surface was modified with phosphate or fluoride (Figure S9a), which is in accordance with the reduction of 4-CP photodegradation rates by HA/TiO_2 in the presence of phosphate or fluoride (Figure S9b). The fluoride or phosphate modification replaces the surface hydroxyl groups with fluoride or phosphate and hinders HA adsorption/complexation onto TiO_2, indicating that light absorption should be related to complexation between TiO_2 and HA. To clarify the photosensitization mechanism responsible for the visible-light photocatalytic activity of HA/TiO_2, the dependence of the rate of 4-CP degradation on the wavelength of incident light was examined. The trend of degradation rates matched well with the LMCT absorption tail, rather than the HA absorption spectrum (inset of Figure 2b). Thus, the TiO_2/HA complex

https://doi.org/10.1021/acs.est.2c02975
Environ. Sci. Technol. 2022, 56, 10829−10837

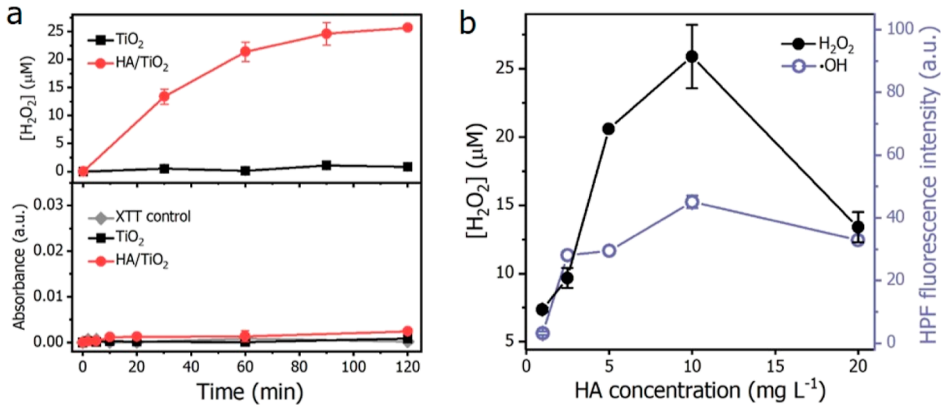

Figure 3. (a) Photocatalytic production of H_2O_2 and XTT-formazan by $O_2^{\bullet-}$ on TiO_2 and HA/TiO_2. (b) Effect of HA concentration on the photocatalytic generation of H_2O_2 and $^{\bullet}OH$ on HA/TiO_2. $^{\bullet}OH$ was measured using the probe HPF. Experimental conditions: [TiO_2] = 0.5 g L^{-1}; [HA] = 10 mg L^{-1}; [XTT]$_0$ = 100 μM; [HPF]$_0$ = 10 μM; pH_i = 3; λ > 420 nm; air-equilibrated.

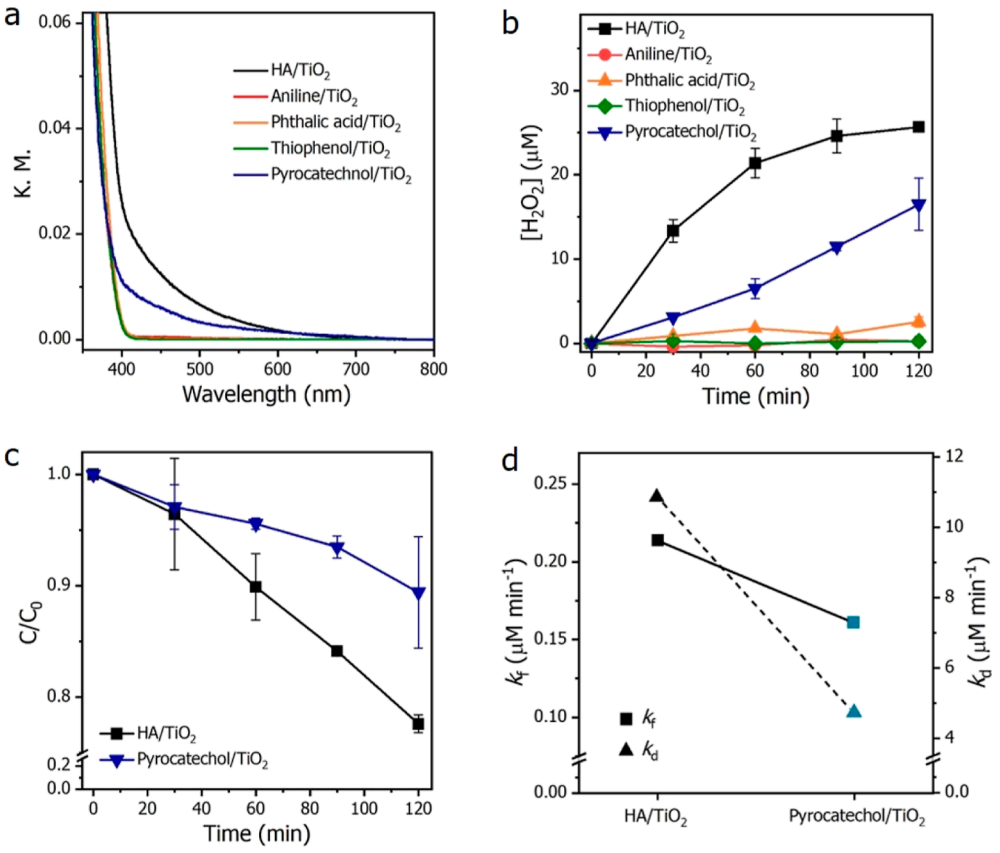

Figure 4. (a) DR UV−vis spectra and (b) photocatalytic H_2O_2 generation of organic ligand/TiO_2. (c) Photocatalytic decomposition of H_2O_2 on HA/TiO_2 and pyrocatechol/TiO_2. (d) Formation rate constant (k_f) and decomposition rate constant (k_d) of H_2O_2 for HA/TiO_2 and pyrocatechol/TiO_2. Experimental conditions: [TiO_2] = 0.5 g L^{-1}; [aniline] = [phthalic acid] = [thiophenol] = [pyrocatechol] = 10 mg L^{-1}; [H_2O_2]$_0$ = 5 mM; pH_i = 3; λ > 420 nm; air-equilibrated.

can induce additional light absorption at λ > 400 nm *via* LMCT and enable enhanced visible-light photocatalytic degradation of 4-CP.

Reaction Mechanism of HA/TiO_2 in Visible Light. Upon visible-light irradiation, photoelectrons generated through the LMCT process are transferred to O_2 to form $O_2^{\bullet-}$. H_2O_2 can be produced by a disproportionation of HO2● (eqs 1 and 2).[33,34]

$$O_2 + e^- \rightarrow O_2^{\bullet-} + H^+ \rightarrow HO_2^{\bullet} \quad (1)$$

$$HO_2^{\bullet} + H^+ + e^- \rightarrow H_2O_2 \quad (2)$$

Figure 3a shows that only a negligible amount of $O_2^{\bullet-}$ was generated upon visible-light irradiation of HA/TiO_2 (at a similar level to XTT control), in contrast to significant production of H_2O_2. While this seems to suggest that H_2O_2 is formed from O_2 reduction rather than $O_2^{\bullet-}$ disproportionation, it may be explained by the short lifetime of $O_2^{\bullet-}$ under acidic conditions and HA—catalyzed $O_2^{\bullet-}$ decay, resulting in lower $O_2^{\bullet-}$ concentrations.[35] Indeed, the typical EPR peak for the DMPO−OOH adduct was observed in Figure S10a,

https://doi.org/10.1021/acs.est.2c02975
Environ. Sci. Technol. 2022, 56, 10829−10837

demonstrating that both uncatalyzed and catalyzed $O_2^{\bullet-}$ decay are involved in H_2O_2 generation. The maximum production of H_2O_2 on HA/TiO_2 was obtained at a HA concentration of 10 mg L^{-1} (Figure 3b), indicating that this is an optimal system-specific concentration that enables strong complexation with TiO_2. To examine $^{\bullet}OH$ production from the decomposition of in situ-generated H_2O_2, changes in the fluorescence intensity of HPF and coumarin−OH adduct (7-hydroxycoumarin, 7-HC) were monitored. Despite much higher fluorescence signals of HPF and 7-HC in HA/TiO_2 than those in TiO_2 (Figure S11), the $^{\bullet}OH$ peaks were not confirmed in the EPR analyses of TiO_2 and HA/TiO_2 (Figure S10b). It is likely that $^{\bullet}OH$ was generated only in low concentration in the HA/TiO_2 system, which is consistent with its inability to degrade DCA (Figure S1). On the other hand, if this result is attributed to $^{\bullet}OH$ scavenging by HA,[36] the amount of $^{\bullet}OH$ generated should decrease as a function of HA concentration. However, a negligible influence of HA concentration (in the range of 2−20 mg/L) on $^{\bullet}OH$ production (Figure 3b) infers that scavenging effects were not significant. Therefore, we do not exclude the possible contribution of $^{\bullet}OH$ in 4-CP degradation but postulate that its contribution is small.

We also verified the role of ROS in 4-CP degradation by employing different radical scavengers, such as CAT for H_2O_2, TBA for $^{\bullet}OH$, and SOD for $^{\bullet}O_2^-$ (Figure S12). Contrary to the weak quenching effect of TBA, significant inhibition was observed in the presence of CAT. Of note, the addition of SOD increased rather than inhibited the degradation, likely due to the greater contribution of H_2O_2 generated from the disproportionation of superoxide by SOD (eq 3) than $O_2^{\bullet-}$ quenching.

$$2O_2^{\bullet-} + 2H^+ \xrightarrow{SOD} O_2 + H_2O_2 \quad (3)$$

Further evidence that *in situ*-generated H_2O_2 acts as a primary reactive species is provided by studies of the oxygen content-dependent degradation. The degradation of 4-CP was almost completely retarded in the O_2-depleted condition (Ar-purged), while it was enhanced in the O_2-saturated condition (Figure S12), a finding consistent with a linear increase in H_2O_2 production with increasing O_2 concentrations (Figure S13).

Role of the HA Functional Group. HA chemistry plays a critical role in driving LMCT complex formation with the TiO_2 surface, and the functional groups −OH, −COOH, −SH, and $-NH_3$ deserve special attention as they are representative of chemistries found in HA.[37] Despite the high chemical heterogeneity of HA, the dominance of carboxylic and phenolic groups over amine and thiol groups is common in a wide variety of HAs.[38] In addition, the functional groups bonded to the benzene ring vary in their electron donating capacities and subsequently influence the optical response.[9] Thus, the relative contribution of each of these functional groups to changes in the optical property of TiO_2 was investigated by systematically varying the functional group-bearing ligands such as pyrocatechol, phthalic acid, thiophenol, and aniline at equivalent doses. The DR UV−vis spectra of the organic ligand/TiO_2 complexes are shown in Figure 4a, where pyrocatechol/TiO_2 revealed a wide range of visible-light absorption, but very little or no absorption was observed for other complexes. Considering that neither pyrocatechol nor TiO_2 responds to visible light (Figure S14), the optical response of the pyrocatechol−TiO_2 complex provides further evidence that LMCT has a role in the visible-light activation of HA/TiO_2 rather than conventional sensitization.

Given that H_2O_2 was the main ROS formed by visible-light-irradiated HA/TiO_2, the visible-light activity of ligand/TiO_2 complexes was tested for H_2O_2 production (Figure 4b). The H_2O_2 production was only evident in the pyrocatechol/TiO_2 complex which showed a pronounced light harvesting capability in the visible range (Figure 4a). Furthermore, pyrocatechol/TiO_2 had a higher degradation efficiency for 4-CP (Figure S15), implying that the in situ-generated H_2O_2 can be involved in the degradation of organic pollutants. Taken together, it seems that the phenolic group-complexed surface is a plausible representation of the active site for visible-light absorption and H_2O_2 production on HA/TiO_2. The higher yield of H_2O_2 on HA/TiO_2 compared to pyrocatechol/TiO_2 might be linked to the stability of the LMCT complex.[12] HA/TiO_2, which would be expected to form a stable LMCT complex on TiO_2 due to the presence of various anchoring groups within the HA, showed a greater magnitude of visible-light absorption than pyrocatechol/TiO_2 (Figure 2b), leading to a higher H_2O_2 production at a given time. Note, however, that a different trend in H_2O_2 production was found between HA/TiO_2 and pyrocatechol/TiO_2. The concentration of H_2O_2 in HA/TiO_2 became saturated after 90 min of irradiation, whereas in pyrocatechol/TiO_2, it increased linearly upon irradiation.

The overall yield of H_2O_2 was determined by the formation and decomposition of H_2O_2 on the TiO_2 surface under visible-light irradiation;[39,40] thus, we tested photocatalytic H_2O_2 decomposition on HA/TiO_2 and pyrocatechol/TiO_2. H_2O_2 was photodegraded more slowly over pyrocatechol/TiO_2 than in the HA/TiO_2 system (Figure 4c). Indeed, when we compared the rates of H_2O_2 formation and decomposition for HA/TiO_2 and pyrocatechol/TiO_2, the formation rate constants were found to be similar to each other, but pyrocatechol/TiO_2 exhibited a lower decomposition rate constant compared to that of HA/TiO_2 (Figure 4d). These results agree with our previous findings that surface functional groups played a different role in enhancing the production of H_2O_2 *via* photocatalysis.[41] Note that although we examine the role of pyrocatechol and other ligands in LMCT sensitization, they represent only a small fraction of the total HA functional groups.

Environmental Implications. Our results demonstrate that the complexation of DOM with the TiO_2 surface leads to visible-light-driven H_2O_2 production, which would enable the degradation of organic pollutants and microbial inactivation. We also confirmed the appreciable production of H_2O_2 by the TiO_2−DOM complex in real river water under simulated sunlight (Figure 5), although the H_2O_2 yield decreased due to the presence of various anions that influence the complexation between TiO_2 and DOM. It is expected that the H_2O_2 concentration generated at commonly reported low TiO_2 concentrations in aquatic systems[42,43] would be below the predicted no-effect concentration of H_2O_2 for aquatic organisms (380 nM).[44] However, in certain areas affected by point sources or urban runoff, there might be relatively high TiO_2 levels (e.g., 150 μg L^{-1} or higher)[45,46] that generate harmful H_2O_2 concentrations. Furthermore, Fenton-like conversion of *in situ*-formed H_2O_2 to the stronger oxidant $^{\bullet}OH$ could occur in the presence of reduced metals [e.g., Fe(II)]. Thus, further research is recommended to examine the dynamics of H_2O_2 formation and decomposition under various

https://doi.org/10.1021/acs.est.2c02975
Environ. Sci. Technol. 2022, 56, 10829−10837

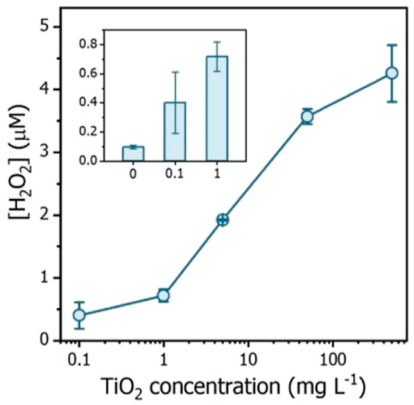

Figure 5. Photogeneration of H_2O_2 in HA-spiked river water samples under solar simulating conditions (AM 1.5 G, 100 mW cm^{-2}) at different TiO_2 concentrations. Experimental condition: [HA] = 10 mg L^{-1}; pH = 7.2 (unadjusted); air-equilibrated.

water chemistry conditions and its effects on the biological activity of aquatic species.

■ ASSOCIATED CONTENT

Supporting Information

The Supporting Information is available free of charge at https://pubs.acs.org/doi/10.1021/acs.est.2c02975.

Schematic illustration of dye sensitization and LMCT sensitization of TiO_2; physicochemical characteristics of the river water sample; PL decay parameters of HA and HA/TiO_2; degradation of DCA under visible light; effect of TBA addition on the degradation of 4-CP under UV and visible-light irradiations; adsorption isotherm of HAs on TiO_2 and zeta potential of TiO_2 and HA as a function of pH; degradation of 4-CP and reduction of Cr(VI) under visible light at pH 6; characterization of HA/TiO_2; PL spectra and nanosecond resolved decay for emission maxima at 550 nm; photocatalytic degradation of HA with TiO_2; DR UV−vis spectra of TiO_2 and HA/TiO_2 at pH 6.6; DR UV−vis spectra and degradation of 4-CP by HA/TiO_2 in the presence of phosphate or fluoride under visible light; EPR spectra; photogenerated $^{\bullet}OH$ detection; effects of scavengers and oxygen content on 4-CP degradation by HA/TiO_2; effect of dissolved oxygen concentration on the photocatalytic production of H_2O_2; UV−vis absorption spectrum of pyrocatechol; and degradation of 4-CP by organic ligand/TiO_2 under visible light (PDF)

■ AUTHOR INFORMATION

Corresponding Authors

Jaesang Lee − *Civil, Environmental, and Architectural Engineering, Korea University, Seoul 02841, Korea;* orcid.org/0000-0001-6642-0225; Phone: +82-2-3290-4864; Email: lee39@korea.ac.kr

Wooyul Kim − *Department of Energy Engineering/ KENTECH Institute for Environmental and Climate Technology, Korea Institute of Energy Technology (KENTECH), Naju 58330, Korea;* orcid.org/0000-0002-8130-5441; Phone: +82- 61-330-9689; Email: wkim@kentech.ac.kr

Eun-Ju Kim − *Water Cycle Research Center, Korea Institute of Science and Technology (KIST), Seoul 02792, Korea;* orcid.org/0000-0001-7700-3240; Phone: +82-2-958-6686; Email: eunjukim@kist.re.kr

Authors

Hoang Tran Bui − *Department of Energy Engineering/ KENTECH Institute for Environmental and Climate Technology, Korea Institute of Energy Technology (KENTECH), Naju 58330, Korea*

Hyeon Yeong Park − *Civil, Environmental, and Architectural Engineering, Korea University, Seoul 02841, Korea; Water Cycle Research Center, Korea Institute of Science and Technology (KIST), Seoul 02792, Korea*

Pedro J. J. Alvarez − *Department of Civil and Environmental Engineering, Rice University, Houston, Texas 77005, United States;* orcid.org/0000-0002-6725-7199

Complete contact information is available at: https://pubs.acs.org/10.1021/acs.est.2c02975

Author Contributions

[⊥]H.T.B. and H.Y.P. contributed equally to this work.

Notes

The authors declare no competing financial interest.

■ ACKNOWLEDGMENTS

This work was supported by the National Research Foundation of Korea (NRF) grant funded by the Korean Government (2022R1A2C2006606 and 2021M3I3A1084818), Risk Assessment Program for Management of Microplastics Project (no. 2020003110004) funded by the Korean Government (MOE) through the KEITI, and Korea Institute of Science and Technology institutional program (2E31932). Partial support for P.J.A.A. was provided by the U.S. National Science Foundation (NSF) ERC on Nanotechnology-Enabled Water Treatment (EEC-1449500).

■ REFERENCES

(1) Sun, T. Y.; Mitrano, D. M.; Bornhöft, N. A.; Scheringer, M.; Hungerbühler, K.; Nowack, B. Envisioning Nano Release Dynamics in a Changing World: Using Dynamic Probabilistic Modeling to Assess Future Environmental Emissions of Engineered Nanomaterials. *Environ. Sci. Technol.* **2017**, *51*, 2854−2863.

(2) Farner, J. M.; Cheong, R. S.; Mahé, E.; Anand, H.; Tufenkji, N. Comparing TiO_2 Nanoparticle Formulations: Stability and Photoreactivity are Key Factors in Acute Toxicity to Daphnia magna. *Environ. Sci.: Nano* **2019**, *6*, 2532−2543.

(3) Park, H.; Park, Y.; Kim, W.; Choi, W. Surface Modification of TiO_2 Photocatalyst for Environmental Applications. *J. Photochem. Photobiol. C Photochem. Rev.* **2013**, *15*, 1−20.

(4) Choi, H.; Stathatos, E.; Dionysiou, D. D. Sol-Gel Preparation of Mesoporous Photocatalytic TiO_2 Films and TiO_2/Al_2O_3 Composite Membranes for Environmental Applications. *Appl. Catal., B* **2006**, *63*, 60−67.

(5) Coelho, L. L.; Hotza, D.; Estrella, A. S.; de Amorim, S. M.; Li Puma, G.; Moreira, R. d. F. P. M. Modulating the Photocatalytic Activity of TiO_2 (P25) with Lanthanum and Graphene Oxide. *J. Photochem. Photobiol., A* **2019**, *372*, 1−10.

(6) Long, M.; Brame, J.; Qin, F.; Bao, J.; Li, Q.; Alvarez, P. J. J. Phosphate Changes Effect of Humic Acids on TiO_2 Photocatalysis: From Inhibition to Mitigation of Electron−Hole Recombination. *Environ. Sci. Technol.* **2017**, *51*, 514−521.

(7) Brame, J.; Long, M.; Li, Q.; Alvarez, P. Inhibitory Effect of Natural Organic Matter or Other Background Constituents on Photocatalytic Advanced Oxidation Processes: Mechanistic Model Development and Validation. *Water Res.* **2015**, *84*, 362−371.

(8) Lee, J.; Mackeyev, Y.; Cho, M.; Li, D.; Kim, J.-H.; Wilson, L. J.; Alvarez, P. J. J. Photochemical and Antimicrobial Properties of Novel C_{60} Derivatives in Aqueous Systems. *Environ. Sci. Technol.* **2009**, *43*, 6604−6610.
(9) Zhang, G.; Kim, G.; Choi, W. Visible Light Driven Photocatalysis Mediated via Ligand-to-Metal Charge Transfer (LMCT): An Alternative Approach to Solar Activation of Titania. *Energy Environ. Sci.* **2014**, *7*, 954−966.
(10) Kim, S.; Moon, G.-h.; Kim, G.; Kang, U.; Park, H.; Choi, W. TiO_2 Complexed with Dopamine-Derived Polymers and the Visible Light Photocatalytic Activities for Water Pollutants. *J. Catal.* **2017**, *346*, 92−100.
(11) Lana-Villarreal, T.; Rodes, A.; Pérez, J. M.; Gómez, R. A Spectroscopic and Electrochemical Approach to the Study of the Interactions and Photoinduced Electron Transfer Between Catechol and Anatase Nanoparticles in Aqueous Solution. *J. Am. Chem. Soc.* **2005**, *127*, 12601−12611.
(12) Zhang, G.; Kim, C.; Choi, W. Poly(4-vinylphenol) as a New Stable and Metal-Free Sensitizer of Titania for Visible Light Photocatalysis through Ligand-to-Metal Charge Transfer Process. *Cat. Today* **2017**, *281*, 109−116.
(13) Park, J.; Moon, G.-h.; Shin, K.-O.; Kim, J. Oxalate-TiO_2 Complex-Mediated Oxidation of Pharmaceutical Pollutants through Ligand-to-Metal Charge Transfer under Visible Light. *Chem. Eng. J.* **2018**, *343*, 689−698.
(14) Weng, Y.-X.; Wang, Y.-Q.; Asbury, J. B.; Ghosh, H. N.; Lian, T. Back Electron Transfer from TiO_2 Nanoparticles to $Fe^{III}(CN)_6^{3-}$: Origin of Non-Single-Exponential and Particle Size Independent Dynamics. *J. Phys. Chem. B* **2000**, *104*, 93−104.
(15) Zhang, Y.; Wang, Z.; Lang, X. Merging Visible Light Photocatalysis of Dye-Sensitized TiO_2 with TEMPO: the Selective Aerobic Oxidation of Alcohols. *Catal.: Sci. Technol.* **2017**, *7*, 4955−4963.
(16) Pelaez, M.; Nolan, N. T.; Pillai, S. C.; Seery, M. K.; Falaras, P.; Kontos, A. G.; Dunlop, P. S. M.; Hamilton, J. W. J.; Byrne, J. A.; O'Shea, K.; Entezari, M. H.; Dionysiou, D. D. A Review on the Visible Light Active Titanium Dioxide Photocatalysts for Environmental Applications. *Appl. Catal., B* **2012**, *125*, 331−349.
(17) Lu, Y.; Yu, H.; Chen, S.; Quan, X.; Zhao, H. Integrating Plasmonic Nanoparticles with TiO_2 Photonic Crystal for Enhancement of Visible-Light-Driven Photocatalysis. *Environ. Sci. Technol.* **2012**, *46*, 1724−1730.
(18) Sandron, S.; Rojas, A.; Wilson, R.; Davies, N. W.; Haddad, P. R.; Shellie, R. A.; Nesterenko, P. N.; Kelleher, B. P.; Paull, B. Chromatographic Methods for the Isolation, Separation and Characterisation of Dissolved Organic Matter. *Environ. Sci.: Processes Impacts* **2015**, *17*, 1531−1567.
(19) Yang, K.; Lin, D.; Xing, B. Interactions of Humic Acid with Nanosized Inorganic Oxides. *Langmuir* **2009**, *25*, 3571.
(20) Varaganti, S.; Ramakrishna, G. Dynamics of Interfacial Charge Transfer Emission in Small Molecule Sensitized TiO_2 Nanoparticles: Is It Localized or Delocalized? *J. Phys. Chem. C* **2010**, *114*, 13917−13925.
(21) Miklos, D. B.; Hartl, R.; Michel, P.; Linden, K. G.; Drewes, J. E.; Hübner, U. UV/H_2O_2 Process Stability and Pilot-Scale Validation for Trace Organic Chemical Removal from Wastewater Treatment Plant Effluents. *Water Res.* **2018**, *136*, 169−179.
(22) Weckhuysen, B. M. In-Situ Characterization of Heterogeneous Catalysts Themed Issue. *Chem. Soc. Rev.* **2010**, *39*, 4557−4559.
(23) Morris, J. J.; Rose, A. L.; Lu, Z. Reactive Oxygen Species in the World Ocean and Their Impacts on Marine Ecosystems. *Redox Biol.* **2022**, *52*, 102285.
(24) Li, F.; Liang, Z.; Zheng, X.; Zhao, W.; Wu, M.; Wang, Z. Toxicity of Nano-TiO_2 on Algae and the Site of Reactive Oxygen Species Production. *Aquat. Toxicol.* **2015**, *158*, 1−13.
(25) Stover, N. M. Diphenylcarbazide as a Test for Chromium. *J. Am. Chem. Soc.* **1928**, *50*, 2363−2366.
(26) Bui, H. T.; Weon, S.; Bae, J. W.; Kim, E.-J.; Kim, B.; Ahn, Y.-Y.; Kim, K.; Lee, H.; Kim, W. Oxygen Vacancy Engineering of Cerium Oxide for the Selective Photocatalytic Oxidation of Aromatic Pollutants. *J. Hazard. Mater.* **2021**, *404*, 123976.
(27) Kormann, C.; Bahnemann, D. W.; Hoffmann, M. R. Photocatalytic Production of Hydrogen Peroxides and Organic Peroxides in Aqueous Suspensions of Titanium Dioxide, Zinc Oxide, and Desert Sand. *Environ. Sci. Technol.* **1988**, *22*, 798−806.
(28) Barbieriková, Z.; Dvoranová, D.; Brezová, V.; Džunuzović, E.; Sredojević, D. N.; Lazić, V.; Nedeljković, J. M. Visible-Light-Responsive Surface-Modified TiO_2 Powder with 4-Chlorophenol: A Combined Experimental and DFT Study. *Opt. Mater.* **2019**, *89*, 237−242.
(29) Kim, G.; Lee, S.-H.; Choi, W. Glucose−TiO_2 Charge Transfer Complex-Mediated Photocatalysis under Visible Light. *Appl. Catal., B* **2015**, *162*, 463−469.
(30) Vatansever, F.; de Melo, W. C. M. A.; Avci, P.; Vecchio, D.; Sadasivam, M.; Gupta, A.; Chandran, R.; Karimi, M.; Parizotto, N. A.; Yin, R.; Tegos, G. P.; Hamblin, M. R. Antimicrobial Strategies Centered Around Reactive Oxygen Species-Bactericidal Antibiotics, Photodynamic Therapy, and Beyond. *FEMS Microbiol. Rev.* **2013**, *37*, 955−989.
(31) Karthik, P.; Vinoth, R.; Selvam, P.; Balaraman, E.; Navaneethan, M.; Hayakawa, Y.; Neppolian, B. A Visible-Light Active Catechol−Metal Oxide Carbonaceous Polymeric Material for Enhanced Photocatalytic Activity. *J. Mater. Chem. A* **2017**, *5*, 384−396.
(32) Jiang, J.; Kappler, A. Kinetics of Microbial and Chemical Reduction of Humic Substances: Implications for Electron Shuttling. *Environ. Sci. Technol.* **2008**, *42*, 3563−3569.
(33) Rao, P. S.; Hayon, E. Redox Potentials of Free Radicals. IV. Superoxide and Hydroperoxy Radicals $^{\bullet}O_2^-$ and $^{\bullet}HO_2$. *J. Phys. Chem.* **1975**, *79*, 397−402.
(34) Zhang, J.; Zheng, L.; Wang, F.; Chen, C.; Wu, H.; Leghari, S. A. K.; Long, M. The Critical Role of Furfural Alcohol in Photocatalytic H_2O_2 production on TiO_2. *Appl. Catal., B* **2020**, *269*, 118770.
(35) Zhang, Y.; Simon, K. A.; Andrew, A. A.; Del Vecchio, R.; Blough, N. V. Enhanced Photoproduction of Hydrogen Peroxide by Humic Substances in the Presence of Phenol Electron Donors. *Environ. Sci. Technol.* **2014**, *48*, 12679−12688.
(36) Brame, J.; Long, M.; Li, Q.; Alvarez, P. Trading Oxidation Power for Efficiency: Differential Inhibition of Photo-generated Hydroxyl Radicals versus Singlet Oxygen. *Water Res.* **2014**, *60*, 259−266.
(37) Adusei-Gyamfi, J.; Ouddane, B.; Rietveld, L.; Cornard, J.-P.; Criquet, J. Natural Organic Matter-Cations Complexation and Its Impact on Water Treatment: A Critical Review. *Water Res.* **2019**, *160*, 130−147.
(38) Zark, M.; Dittmar, T. Universal Molecular Structures in Natural Dissolved Organic Matter. *Nat. Commun.* **2018**, *9*, 3178.
(39) Li, X.; Chen, C.; Zhao, J. Mechanism of Photodecomposition of H_2O_2 on TiO_2 Surfaces under Visible Light Irradiation. *Langmuir* **2001**, *17*, 4118−4122.
(40) Lee, T.; Bui, H. T.; Yoo, J.; Ra, M.; Han, S. H.; Kim, W.; Kwon, W. Formation of TiO_2@carbon Core/Shell Nanocomposites from a Single Molecular Layer of Aromatic Compounds for Photocatalytic Hydrogen Peroxide Generation. *ACS Appl. Mater. Interfaces* **2019**, *11*, 41196−41203.
(41) Gu, M.; Lee, D.-Y.; Mun, J.; Kim, D.; Cho, H.-i.; Kim, B.; Kim, W.; Lee, G.; Kim, B.-S.; Kim, H.-i.; Kim, H. Solar-to-Hydrogen Peroxide Conversion of Photocatalytic Carbon Dots with Anthraquinone: Unveiling the Dual Role of Surface Functionalities. *Appl. Catal., B* **2022**, *312*, 121379.
(42) Shi, X.; Li, Z.; Chen, W.; Qiang, L.; Xia, J.; Chen, M.; Zhu, L.; Alvarez, P. J. J. Fate of TiO_2 Nanoparticles Entering Sewage Treatment Plants and Bioaccumulation in Fish in the Receiving Streams. *NanoImpact* **2016**, *3*−*4*, 96−103.
(43) Loosli, F.; Wang, J.; Rothenberg, S.; Bizimis, M.; Winkler, C.; Borovinskaya, O.; Flamigni, L.; Baalousha, M. Sewage Spills Are a Major Source of Titanium Dioxide Engineered (Nano)-Particle Release into the Environment. *Environ. Sci.: Nano* **2019**, *6*, 763−777.

(44) Sunday, M. O.; Jadoon, W. A.; Ayeni, T. T.; Iwamoto, Y.; Takeda, K.; Imaizumi, Y.; Arakaki, T.; Sakugawa, H. Heterogeneity and Potential Aquatic Toxicity of Hydrogen Peroxide Concentrations in Selected Rivers Across Japan. *Sci. Total Environ.* **2020**, *733*, 139349.
(45) Polesel, F.; Farkas, J.; Kjos, M.; Almeida Carvalho, P.; Flores-Alsina, X.; Gernaey, K. V.; Hansen, S. F.; Plósz, B. G.; Booth, A. M. Occurrence, Characterisation and Fate of (Nano)Particulate Ti and Ag in Two Norwegian Wastewater Treatment Plants. *Water Res.* **2018**, *141*, 19−31.
(46) Kaegi, R.; Ulrich, A.; Sinnet, B.; Vonbank, R.; Wichser, A.; Zuleeg, S.; Simmler, H.; Brunner, S.; Vonmont, H.; Burkhardt, M.; Boller, M. Synthetic TiO_2 Nanoparticle Emission from Exterior Facades into the Aquatic Environment. *Environ. Pollut.* **2008**, *156*, 233−239.

https://doi.org/10.1021/acs.est.2c02975
Environ. Sci. Technol. 2022, 56, 10829−10837